J Nanopart Res (2013) 15:1698
DOI 10.1007/s11051-013-1698-y

RESEARCH PAPER

Composite polyester membranes with embedded dendrimer hosts and bimetallic Fe/Ni nanoparticles: synthesis, characterisation and application to water treatment

S. P. Malinga · O. A. Arotiba · R. W. M. Krause · S. F. Mapolie · M. S. Diallo · B. B. Mamba

Received: 27 November 2012 / Accepted: 4 May 2013 / Published online: 21 May 2013

Abstract This study describes the preparation, characterization and evaluation of new composite membranes with embedded dendrimer hosts and Fe/Ni nanoparticles. These new reactive membranes consist of films of cyclodextrin–poly(propyleneimine) dendrimers (β-CD–PPI) that are deposited onto commercial polysulfone microporous supports and crosslinked with trimesoyl chloride (TMC). The membranes were subsequently loaded with Fe/Ni nanoparticles and evaluated as separation/reactive media in aqueous solutions using 2,4,6-trichlorophenol as model pollutant. The morphology and physicochemical properties of the composite membranes were characterised using high-resolution transmission electron microscopy (HR-TEM), atomic force microscopy and measurements of contact angle, water intake, porosity and water permeability. The sorption capacity and catalytic activity of the membranes were evaluated using ion chromatography, atmospheric pressure chemical ionisation-mass spectrometry and UV–Vis spectroscopy (UV–Vis). The sizes of the embedded Fe/Ni nanoparticles in the membranes ranged from 40 to 66 nm as confirmed by HR-TEM. The reaction rates for the dechlorination of 2,4,6-trichlorophenol ranged from 0.00148 to 0.00250 min^{-1}. In all cases, we found that the reaction by-products consisted of chloride ions and mixtures of compounds including phenol ($m/z = 93$), 2,4-dichlorophenol ($m/z = 163$)

Special Issue Editors: Mamadou Diallo, Neil Fromer, Myung S. Jhon

This article is part of the Topical Collection on Nanotechnology for Sustainable Development

Electronic supplementary material The online version of this article (doi:10.1007/s11051-013-1698-y) contains supplementary material, which is available to authorized users.

S. P. Malinga (✉) · O. A. Arotiba · M. S. Diallo · B. B. Mamba
Department of Applied Chemistry, University of Johannesburg, P.O. Box 17011, Doornfontein 2028, South Africa
e-mail: sitholespr@yahoo.com

B. B. Mamba
e-mail: bmamba@uj.ac.za

R. W. M. Krause
Department of Chemistry, Rhodes University, P.O. Box 94, Grahamstown 6140, South Africa

S. F. Mapolie
Department of Chemistry and Polymer Science, University of Stellenbosch, Private Bag X1, Matieland 7602, South Africa

M. S. Diallo
Graduate School of EEWS, Korea Advanced Institute of Science and Technology (KAIST), Daejeon 305-701, Republic of Korea

M. S. Diallo
Division of Engineering and Applied Science, Environmental Science and Engineering, California Institute of Technology, Pasadena, CA 91125, USA

and 4-chlorophenol ($m/z = 128$). The overall results of this study suggest that β-CD–PPI dendrimers are promising building blocks for the synthesis of composite and reactive membranes for the efficient removal of chlorinated organic pollutants from water.

Keywords β-Cyclodextrin · Fe/Ni nanoparticles · Poly(propyleneimine) dendrimer · Polysulfone · 2,4,6-Trichlorophenol

Introduction

Membranes have gained a lot of attention in the chemical technology industry and these have been used in a wide range of applications such as the production of high quality water, removal and recovery of toxic and valuable components from industrial effluent (Abedini et al. 2011). The introduction of membrane technology in separation and concentration has become industrially viable due to the low energy of operation, high efficiency of separation and simplicity of operation (Abedini et al. 2011). Traditionally, membranes have been used in separation based on size exclusion, solution diffusion or Donnan exclusion (Smuleac et al. 2010). However, the fabrication of membranes with novel materials such as nanostructured dendrimer–cyclodextrin (Fig. 1a) Ni–Fe bimetalics can extend their application towards advanced separation and catalysis.

Dendrimers are highly branched, globular, nanoscopic macromolecules with numerous terminal groups (Sarkar et al. 2010). Dendrimers have been regarded as high performance material over the past decade and have received greater attention due to their exquisite structure have found many possible applications in the field of catalysis, drug delivery and biomimetics (Lianchao et al. 2006; Wei et al. 2008). Poly(propyleneimine) (PPI) dendrimers are macromolecules with three-dimensional structures which consist of an interior diaminobutane core, interior branching units (propylene imine) and peripheral functional groups (NH_2 groups in the unfunctionalised polymer) (Vassilev et al. 2009). The use of dendrimers in bimetallic and monometallic nanoparticle synthesis is well established and this has led to the production of nanoparticles which are cone-, spherical- or disc-like shaped, soft and have very low polydispersity and sizes in the range of 1–3 nm (Diallo et al. 2005; Bao et al. 2003; Weir et al. 2010; Scott et al. 2004). A number of key factors make dendrimers particularly interesting in nanoparticle and macromolecular synthesis. First, dendrimers have a high number of internal amine functional groups, which can act as ligands to complex metal ions such as Cu, Fe, Ag and Ni for nanoparticle synthesis (Huang et al. 2008; Diallo et al. 2005). Second, the presence of nanocavities in the dendrimer structure acts as hosts/templates for the preparation of narrow and stable nanoparticles (Bai et al. 2009). The quasispherical hyperbranched structure of the dendrimers (generation 4 and above) also provides a shell to prevent aggregation of the nanoparticles (Huang et al. 2008). Third, the nanocavities can act as catalytic and adsorption sites for the degradation and removal of organic pollutants. Lastly, the highly branched peripheral amine functional groups can be grafted with other molecules (such as cyclodextrins) to prepare a new generation of multifunctional material. The incorporation of β-cyclodextrin to dendrimers provides a unique polymer structure that exhibits the combination of the two-type of molecular cavities as well as characteristics of both the cyclodextrin and the dendrimer (Fig. 1a) (Li et al. 2011).

Recent advances in membrane research such as the fabrication of nanoparticles within structures has been reported. Lee et al. (2008) fabricated a novel polyamide nanocomposite membrane containing TiO_2 nanoparticles synthesised via in situ polymerisation. The membrane was found to have very high rejection towards $MgSO_4$ (95 %) and a permeate flux of 9.1 L m^{-2} h^{-1}. Smuleac and co-workers (2010; 2011) prepared Fe/Pd nanoparticles in a polymer film consisting of polyacrylic acid coated on a polyvinylidene fluoride membrane for the degradation of trichloroethylene and 2,2-dichlorobiphenyl. The inclusion of Fe/Pd bimetallic system into the polymeric film was found to improve the degradation rate from 0.005 (for Fe only) to 0.008 L m^{-2} h^{-1} when Fe/Pd bimetallic system was used for the degradation of trichloroethylene (Smuleac et al. 2010). On the other hand, 2,2-dichlorophenyl was converted to phenyl in <40 s (Smuleac et al. 2010).

Despite these promising results a great deal of work still needs to be done to develop more efficient technologies to extract clean water from industrial runoff, wastewater and sea water. Thus, in this study, a new generation of multifunctional membranes

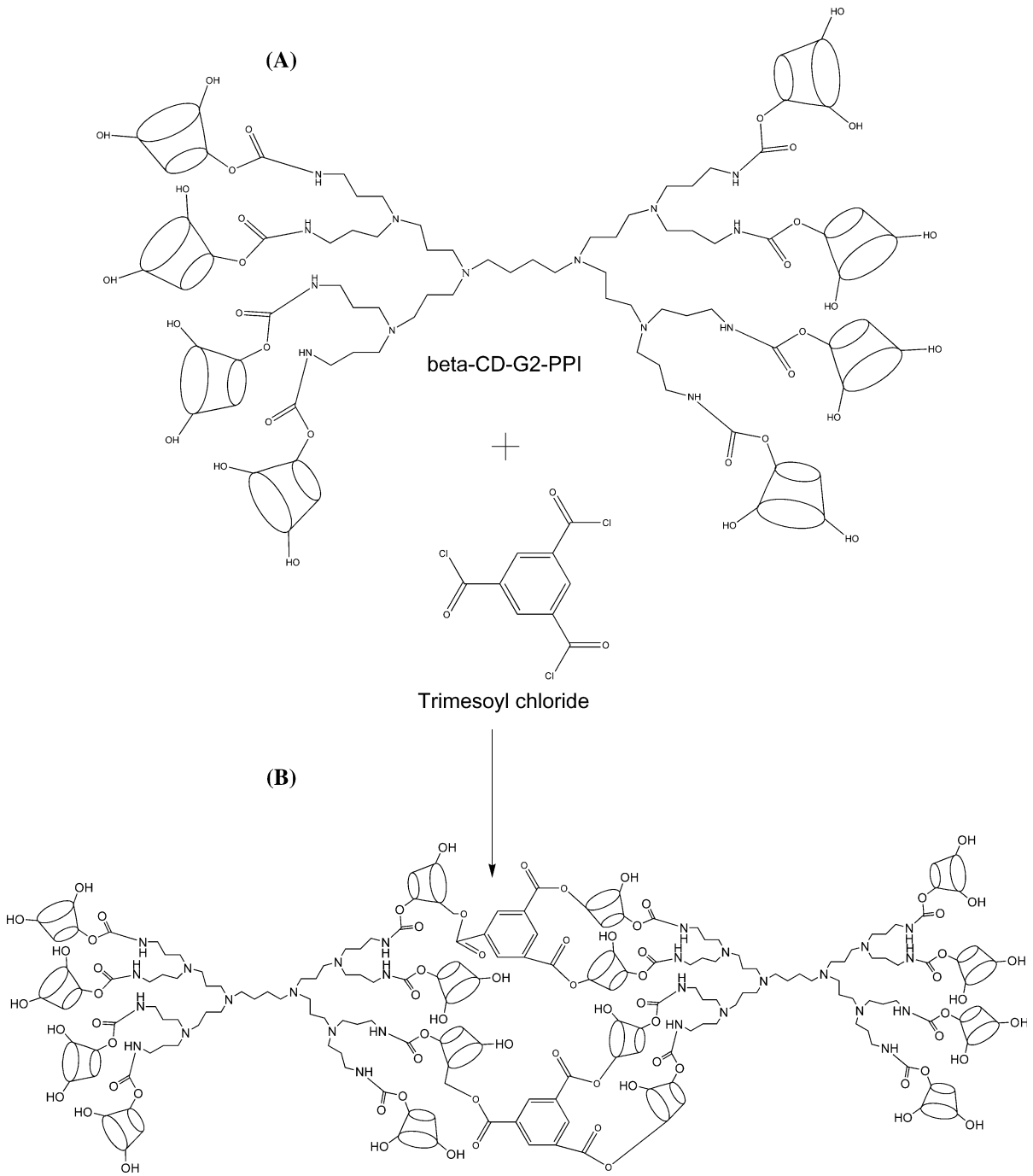

Fig. 1 β-CD–G2-PPI (**a**) reaction with trimesoyl chloride to produce a highly crosslinked β-CD–G2-PPI structure (**b**)

embedded with β-cyclodextrin–poly(propyleneimine) dendrimer and catalytic Ni/Fe centres were prepared and used to carry out both catalysis and adsorption. Specifically, β-cyclodextrin and generation 3 (G3)/ generation 4 (G4) poly(propyleneimine) (PPI) (β-CD–G3 and β-CD–G4) were incorporated on polysulfone (PSf) as a coating layer to form a thin film composite using trimesoyl chloride. These membranes (β-CD–G3-PSf and β-CD–G4-PSf) were then dip coated in Fe and Ni solution followed by metal reduction using

$NaBH_4$ to prepare the catalytic membranes (β-CD–G3-PSf-Fe/Ni and β-CD–G4-PSf-Fe/Ni). The synthesis of Ni/Fe bimetallic system in a β-cyclodextrin–dendrimer PSf domain has not been reported before. To further demonstrate the usefulness of these membranes, the membranes were applied in the dechlorination and adsorption of 2,4,6-trichlorophenol (TCP).

Experimental methods and procedures

Materials

Generation 3 (G3) and generation 4 (G4) poly(propylene imine) dendrimers were purchased from SyMO-Chem B.V (Netherlands). *N,N*-carbonyldiimidazole(CDI) was purchased from Sigma Aldrich (USA). The purification of the β-CD–dendrimer conjugates was carried out using benzoylated dialysis tubing with molecular weight cut off of 1,200 g mol^{-1}, from Sigma, Aldrich (USA). Commercial ultrafiltration flat sheet of PSf membrane was supplied by Marsi water (Pty) Ltd (Northriding, South Africa). 1,3,5-Benzenetricarbonyl trichloride (TMC) and *N*-(3-dimethylamino propyl)-*N*-ethyl-carbodiimide hydrochloride (EDC) were purchased from Sigma Aldrich Company (St. Louis, USA). 2,4,6-Trichlorophenol, Ni (II) nitrate hexahydrate (Ni $(NO_3)_2{\cdot}6H_2O$), Ferric nitrate (Fe $(NO_3)_3{\cdot}9H_2O$) and sodium borohydride were purchased from Fluka. All chemicals and materials were used as received.

Host synthesis (β-CD–PPI)

A typical conjugation reaction of precursor β-cyclodextrin carbonylimidazole and poly(propyleneimine) dendrimer (generations 3 and 4) was carried out as follows: generation 3 poly(propyleneimine) (G3-PPI) (0.211 g, 0.125 mmol) was dissolved in dimethylsulphoxide (3 mL); β-cyclodextrin imidazole (2.446 g, 1.9 mmol) and triethylamine (3 mL) were added to this dendrimer solution. This solution was stirred at room temperature for 24 h and purified using dialysis against deionised water for 2 days. Lyophilization of the solution for 2 days resulted in a white fluffy solid. A similar procedure was used for the preparation of β-CD–G4-PPI host. Figure 1a shows an example of the host material β-CD–G2-PPI (i.e., 8 β-CD molecules). For β-CD–G3-PPI and β-CD–G4-PPI, 16 and 32 β-CD molecules are attached to the periphery, respectively. Figures S1, S2, S3 and S4 show the FTIR, HNMR and MS–ESI analysis, respectively, confirming that the host structure was successfully synthesised.

Membrane synthesis

The membranes were prepared using an interfacial polymerisation reaction. The aqueous phase solution was prepared by dissolving β-cyclodextrin–poly(propyleneimine) (β-CD–PPI) (6 %, w/v) (generation 3 or 4) in water. The microporous commercial PSf membrane was then dip coated in the aqueous solution for 24 h at room temperature. The residual liquid was drained and *N*-(3-dimethylamino propyl)-*N*-ethyl-carbodiimide hydrochloride solution (5 % w/v) in a phosphate buffer solution (pH = 5.6) was poured over the membrane and left to react for 3 h. This solution was used as a coupling agent to promote esterification. The membrane was then placed in the organic phase, i.e., trimesoyl chloride (1 % w/v) in n-hexane and the reaction time was set to 60 s. The membrane was dried in the oven at 60 °C for 30 min to promote further polymerisation. The modified PSf membranes were then washed with deionised water to remove any residual trimesoyl chloride and stored in deionised water. The reaction between the host (β-CD–G2-PPI) and trimesoyl chloride generates a crosslinked structure shown in Fig. 1b. Figure S5 shows FTIR analysis of the membrane confirming successful crosslinking of the β-CD–PPI host with trimesoyl chloride to give a polyester membrane.

Preparation of Fe/Ni-modified membranes

Prior to the Fe/Ni nanoparticle preparation, the membranes were immersed in NaCl (5 wt%) solution (pH = 10) overnight to deprotonate the hydroxyl groups (Smuleac et al. 2010). The deprotonation was carried out to facilitate metal binding with the membrane. The membrane was thoroughly washed with deionised water until the pH became neutral. It was then immersed in an aqueous solution containing $NiNO_3{\cdot}9H_2O$ (2.4 wt%) and $FeNO_3{\cdot}9H_2O$ (7.8 wt%) and shaken overnight to provide efficient deposition of the metal ions onto the membrane. Argon was purged into the solution to prevent oxidation. The encapsulated Fe^{2+}/Ni^{2+} ions were simultaneously reduced with

aqueous $NaBH_4$ (0.4 M, 25 mL) for 20 min and this resulted in the catalytic membrane (Xu et al. 2005). The membrane was stored in ethanol to prevent oxidation.

Membrane characterisation

Fourier transform infrared-attenuated total reflection (FTIR-ATR)

The membrane samples were analysed with a Perkin Elmer 100 FTIR spectrophotometer. Powder and membranes samples (with active side facing down) were placed on the ATR and analysed in the range 650–4,000 cm^{-1} averaging 32 scans at a spectral resolution of 4 cm^{-1}.

Atomic force microscopy (AFM)

Multimode Atomic Force Microscope (Nano Scope Version (IV) was used to determine surface morphology and roughness (Rq) of the membranes. The membrane sample (1 cm × 1 cm) was placed on a sample holder and a RTESPW tip with a radius of curvature of <10 nm (Veeco instruments) was used. The tip was mounted on a 125-μm-long cantilever with the spring constant of 40 N/m and this was employed for the tapping mode experiment. The height and phase images were obtained using a scan rate of 0.5 Hz and the tip frequencies ranged from 280 to 310 kHz.

Scanning electron microscopy (SEM)

Scanning electron microscopy was used to determine the cross-sectional images of the thin film composite. The samples were frozen and fractured in liquid nitrogen, coated with carbon and mounted on the instrument. The samples were then examined using Field emission scanning electron microscopy (Joel, JSM, 7500F).

Contact angle analysis

Contact angle analyses were measured using the sessile drop method with a Data Physics optical contact angle instrument. About ten measurements were conducted at different sites per sample and all measurements were recorded at room temperature. These analyses were carried out in order to determine the hydrophilicity of the membranes.

High-resolution transmission electron microscopy (HR-TEM)

The membrane samples were prepared by sectioning with a diamond knife to give very thin sections. These thin sections were examined using HRTEM JOEL JEM-2100 coupled to an energy dispersive X-ray spectroscopy (EDS).

Water intake capacity and porosity measurements

Water intake capacity was performed to evaluate the adsorption of water by the fabricated membranes. The water intake capacity of the membrane was obtained after soaking the membrane in deionised water for 24 h. The membranes were weighed after mopping with paper to obtain the wet weight. The membranes were dried in an oven at 60 °C for 24 h to obtain the dry weight. The percent water intake capacity (WIC) was calculated using Eq. (1) (Adams et al. 2012);

$$\mathrm{WIC}(\%) = \frac{W_w - W_d}{W_w} \times 100 \quad (1)$$

where w_w and w_d are the wet and dry weights of the membrane, respectively.

Membrane porosity was determined by immersing the membrane in water for 24 h followed by blotting the membrane with paper and the wet weight of the membrane was measured. The membrane was dried in an oven at 60 °C for 24 h and the weight was measured again. The porosity of the membrane (P) was measured by using Eq. 2 (Adams et al. 2012):

$$P(\%) = \frac{(W_0 - W_1)}{Ah} \times 1000 \quad (2)$$

where w_0 and w_1 are the weight of the wet and dry membrane, respectively, A is the area of the membrane (cm^2) and h is the membrane thickness (mm).

Membrane performance evaluation

The separation performance tests for β-CD–PPI–PSf, β-CD–PPI–PSf-Fe/Ni and native PSf membranes were carried using a six-cell crossflow parallel membrane system shown in Scheme 1. The membranes were stabilised with distilled water at 2.4 MPa for 2 h with deionised water before testing. The six-cell crossflow system has a set of membrane cells fed in parallel from a single feed tank (Jin et al. 2009). The water in the

feed tank was maintained by magnetic stirring and was pressurised into the system by a hydra cell pump. A laboratory recirculating heater chiller (Poly Science digital temperature controller) maintained the feed water at 22 °C. Back pressure regulators (Swagelok) and bypass valves controlled the feed water hydraulic pressure and crossflow velocity for each side individually (Jin et al. 2009). After sampling, the permeate and retentate were returned to the feed tank in order to maintain a constant concentration of 2,4,6-TCP.

The membrane permeability was determined from pure water flux using deionised water. The water flux was (J_w) is expressed in Eq. 3 (Adams et al. 2012):

$$J_w = \frac{V}{At} \tag{3}$$

where v is the permeate volume (m^3), A is the effective membrane area (0.00129 m^2) and t is the time (hours) to collect the permeate volume. To evaluate the dechlorination performance of the membrane towards 2,4,6-TCP, the feed solution (50 mg $L^{-1)}$ was passed through the membrane at a pressure of 0.69 MPa. The permeate was collected at constant time intervals and analysed using an UV–Vis spectrophotometer at 293 nm. The amount of 2,4,6-TCP adsorbed per unit area of the membrane was calculated using Eq. 4:

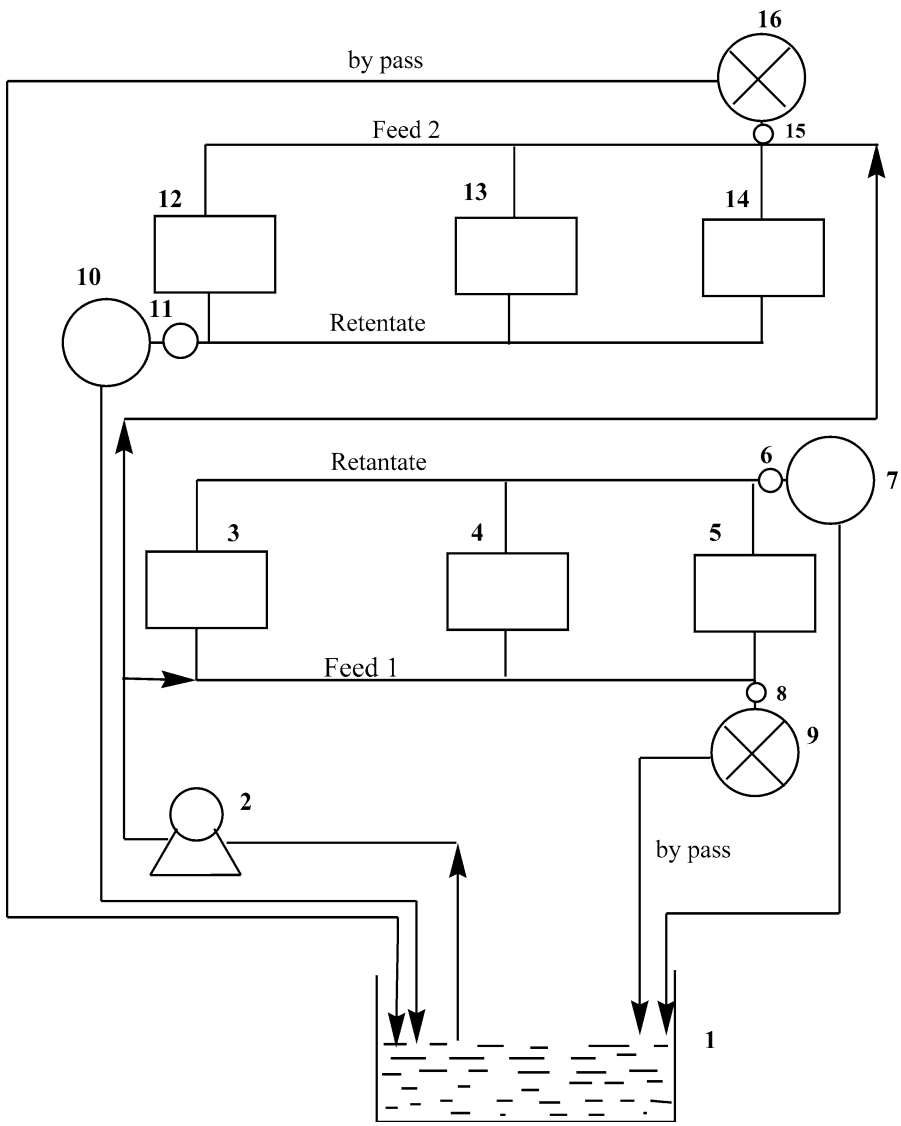

Scheme 1 A schematic representation of a six-cell crossflow system (*1*) feed solution (10 L, 22 °C), (*2*) feed pump (*3–5*), and (*12–14*) membrane cell, (*6* and *11*) back pressure regulators, (*7* and *10*) flow meter, (*8* and *15*) by pass valves, (*9* and *16*) pressure gauges

$$\text{TCP adsorption} = \frac{C_f - C_p}{A} \times V \quad (4)$$

where c_p is the concentration of the permeate, c_f is the concentration of the feed (mg L^{-1}), A is the membrane area in cm^2 and V is the total volume of the solution (L).

Batch analysis for evaluation of kinetics

Membranes containing Fe/Ni nanoparticles were immersed in a sealed erlenmeyer flask containing 2,4,6-triclorophenol (50 mg L^{-1}) solution under argon gas. This solution was shaken on a shaker at a speed of 180 rpm. The samples were collected at different time intervals using a syringe and analysed using an UV–Vis spectrophotometer at 293 nm.

Ion chromatography analysis

The concentration of chlorine ions was determined using Ion chromatography (Dionex ICS-2000 equipped with a Dionex Ionpac AS18 (2 × 250 mm) column) and the samples were first filtered through polyvinylidene fluoride syringe filters (0.45 μm) before analysis.

Atmospheric pressure chemical ionisation-mass spectrometry (APCI-MS) analysis

The dechlorination by-products (2,4-dichlorophenol, 4-chlorophenol and phenol) were analysed by liquid chromatography–mass spectrometry (Waters e2695, Separations). A methanol (80 %):water (20 %) mobile phase was used and the injection volume was set at 1 μL using direct infusion.

Results and discussion

HR-TEM analysis

The morphology of Fe/Ni nanoparticles was determined by HR-TEM cross-sectional images illustrated in Fig. 2a, c. The TEM micrographs illustrate that the nanoparticles were uniformly and densely dispersed within the structure of the membrane. The particle sizes ranged from 59 to 66 nm for β-CD–G3-Ni/Fe and 47–58 nm for β-CD–G4-PSf-Ni/Fe. The mean diameters of the synthesised nanoparticles were 66 nm (Fig. 2b) and 59 nm (Fig. 2d) for β-CD–G3-Fe/Ni and β-CD–G4-PSf-Fe/Ni, respectively. The corresponding EDS (Fig. 2e) affirmed the presence of Fe/Ni within the membranes; the Ni and Fe were detected at 7.5 and 6.2 keV, respectively. Xu et al. (2005) also observed the same EDS line profile for Fe/Ni synthesised in polyacrylic acid/polyethersulfone membranes. The synthesised nanoparticles were bigger in size than the Fe/Ni nanoparticles individually prepared in generation 2 and generation 3 poly(propyleneimine) dendrimers which were in the quantum dot size range (1–4 nm) (Malinga et al. 2012). In this nanoparticle range, the Fe/Ni nanoalloy is said to have been formed inside the dendrimer cavities. In a similar study by Meyer and Bhattacharyya (2007) where Fe/Ni was imbedded on cellulose acetate membrane the particle sizes were found to range from 18 to 80 nm within the membrane cross-section. Formation of large nanoparticles sizes after synthesis in membranes has been reported is attributed to the fact that membranes have a more open structure (Meyer and Bhattacharyya 2007). Fe/Pd nanoparticles were also synthesised in polyacrylic acid embedded in a polyvinylidene fluoride membrane and these nanoparticles were reported to be in the range of 20–30 nm (Smuleac et al. 2010). However, the Fe/Ni nanoparticles synthesised in this study were still in the nanometer range (1–100 nm). EDS mapping shown in Fig. S6 gave evidence that the Fe and Ni were distributed uniformly in the membrane therefore bimetallic Fe/Ni nanoparticles were fabricated within the membranes.

AFM analysis

The surface morphology of the membranes were further characterised by AFM. The AFM topography and roughness measurements revealed that the change in roughness was a result of various membrane fabrication processes. In general, the morphology of the membranes changes after coating with cyclodextrin–dendrimer material followed by subsequent loading of Fe/Ni nanoparticles (Fig. 3b–e) as compared to the unmodified PSf (Fig. 3a). There is appearance of protrusions which form a ridge and valley structures and these morphological changes are complemented by the increase in roughness measurements observed in Fig. 4. The roughness increased in the following sequence: PSf < β-CD–G3-PSf and β-CD–G4-PSf < β-CD–G3-PSf-Fe/Ni and β-CD–G4-PSf-Fe/Ni. Wei et al. (2008) also found that the roughness

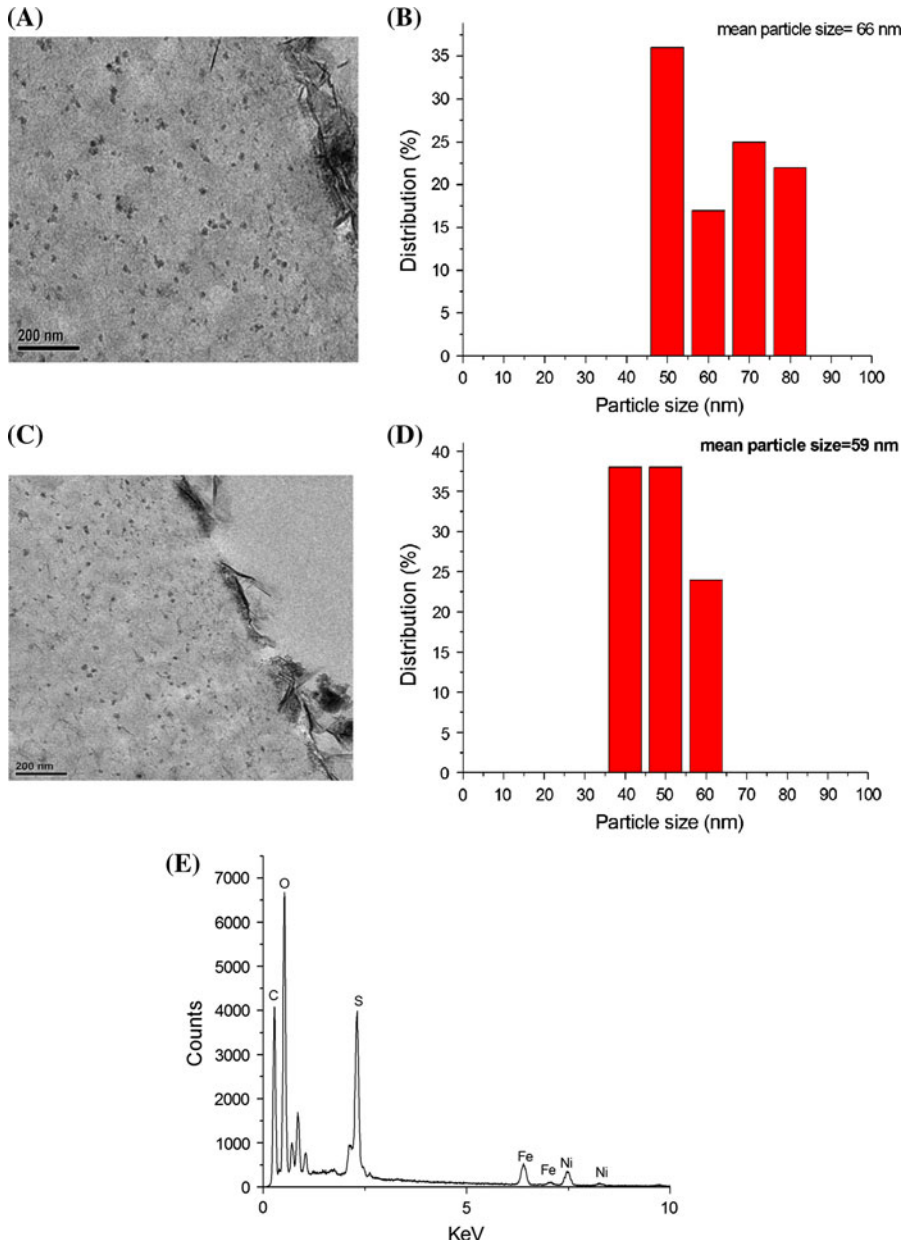

Fig. 2 HR-TEM for **a** β-CD–G3-PSf-Fe/Ni and **b** corresponding size distribution histogram. **c** β-CD–G4-PSf-Fe/Ni and **d** corresponding size distribution histogram. **e** EDS spectrum

increased after each fabrication process step, i.e., PSf–ultrafiltration membrane (5.5 nm) to PSf–ethanol membrane (5.7 nm) and finally PSf–hyperbranched polyether membranes (6.5–12.5 nm).

Water intake capacity, contact angle and pure water flux

Figure 5 shows that generally the water flux increased with increasing operating pressure and the water permeability was calculated using the four different applied pressures. Table 1 shows the water intake capacity, contact angle, porosity and pure water permeability of the β-CD–PPI–PSf with Fe/Ni nanoparticles. After nanoparticle incorporation of the β-CD–G3/G4-PSf membrane, the pure water permeability was found to decrease from 26 to 20 m h^{-1} MPa^{-1} for β-CD–G3-PSf-Fe/Ni and from 46 to 16 m h^{-1} MPa^{-1} for β-CD–G4-PSf-Fe/Ni. Introduction of the nanoparticle in the membrane matrix reduced pure

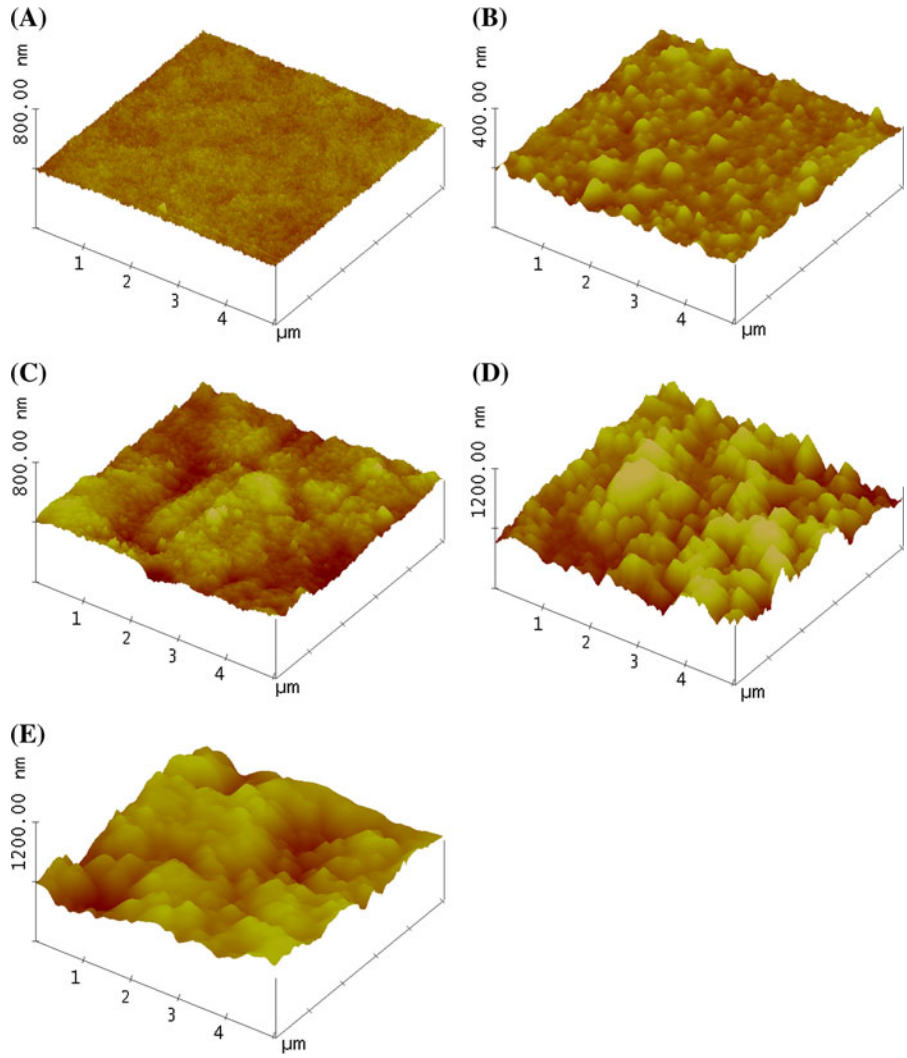

Fig. 3 AFM images of **a** Commercial PSf, **b** β-CD–G3-PSf, **c** β-CD–G4-PSf, **d** β-CD–G3-PSf-Fe/Ni, **e** β-CD–G4-PSf-Fe/Ni

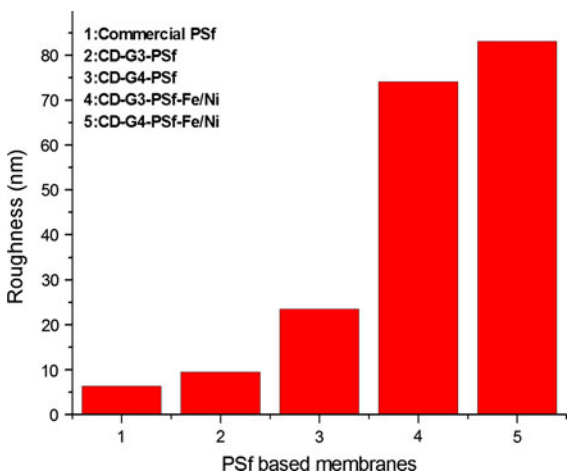

Fig. 4 Roughness of PSf-based membranes

water permeability. It also had a slight effect in the porosity and water content. This trend was also reported by Xu et al. (2005) when Fe/Ni nanoparticles were synthesised on polyacrylic acid polyether sulfone composite membrane. The pure water permeability of the polyacrylic acid/polyethersulfone (PAA/PES) with Fe/Ni had the lowest pure water permeability (0.27×10^{-4} cm^3 cm^{-2} bar^{-1} s^{-1}) as compared to the PAA/PES (3.03×10^{-4} cm^3 cm^{-2} bar^{-1} s^{-1}) and PES (76.9×10^{-4} cm^3 cm^{-2} bar^{-1} s^{-1}) (Xu et al. 2005). This was attributed to the resistance from the PAA coating layer and Fe/Ni immobilised in the membrane which affects the membrane pore matrix thus reducing the membrane pore size and porosity as demonstrated by our results (Table 1) (Xu et al. 2005). Smuleac et al. (2010) also obtained similar results

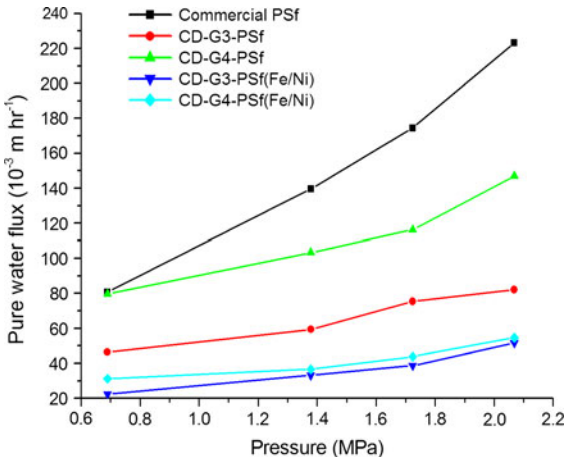

Fig. 5 The relationship between pure water flux and pressure

where the membrane permeability was found to decrease after each functionalisation step. The water permeability of bare polyvinylidene fluoride membrane was 4,824 $\times$ 10^{-4} cm^3 cm^{-2} s^{-1} bar^{-1} which decreased after the addition of iron to 468.7 $\times$ 10^{-4} cm^3 cm^{-2} s^{-1} bar^{-1}. Liu et al. (2010) also observed that as more components or layers are added to the membrane the pure water flux gradually decreases. In this study, crosslinking of the base membrane chitosan with activated carbon fibre and then dip coating in TiO_2 reduced the water flux from 34.35 to 19.56 m^3 m^{-2} h^{-1} (Liu et al. 2010). As illustrated in Table 1, there is decrease in permeability as components are introduced to the base PSf membrane. This is because the addition of nanoparticles reduces the membrane pore voids resulting in increase in resistance to water permeation. The membranes coated with nanoparticles maintained their hydrophilicity as the contact angle remained below that of PSf membrane.

Adsorptive removal of 2,4,6-trichlorophenol from water using PSf, β-CD–G3-PSf and β-CD–G4-PSf

Figure 6a shows 2,4,6-trichlorophenol adsorption of the base membrane (PSf), β-CD–G3-PSf and β-CD–G4-PSf. The removal efficiency of all the modified membranes was higher as compared to the PSf. As the reaction progressed the removal efficiencies decreased and reached a steady state. The modified membranes exhibit cyclodextrin–dendrimer nanocavities which can efficiently adsorb and encapsulate organic pollutants such as 2,4,6-trichlorophenol and this network system is present in all the membranes tested except PSf. In a study conducted by Li et al. (2011), polyamidoamine–cyclodextrin (PAMAM–CD) copolymer was found to have high adsorption efficiencies towards organic compounds such as 2,4,6-trichlorophenol (up to 92 %), 2,4-dichlorophenol (69 %) and poceau 4R (up to 99.6 %). It was concluded that these adsorbents were adsorbed to a large extent onto the surface or into the PAMAM–CD through interactions with nitrogen and oxygen available within the PAMAM–CD copolymer (Li et al. 2011). The high removal efficiency of modified membranes could be due to the interaction of 2,4,6-TCP with the nitrogen and oxygen available from the poly(propyleneimine)–cyclodextrin structure (Fig. 1a) which are active sites on the surface and within β-cyclodextrin–poly(propyleneimine) conjugate.

The corresponding solute fluxes of the membranes are depicted in Fig. 6b. The modified β-CD–PPI–PSf-Fe/Ni membranes exhibited a lower flux than β-CD–PPI–PSf and native PSf and this was attributed to the increase in the thickness of the thin film layer. The thickness of the selective layer estimated using Imagej software (Park et al. 2012) from the cross-section SEM images are shown in Fig. 7. The thickness of the film was found to be 45 and 39 μm β-CD–G3-PPI–PSf and β-CD–G4-PPI–PSf, respectively. Upon addition of Fe/Ni nanoparticle, the layer thickness increased to 259 μm for β-CD–G3-PPI–PSf-Fe/Ni and 109 μm for β-CD–G4-PPI–PSf-Fe/Ni. According to Singh et al. (2011), composite membranes which have a thicker selective layer exhibit a lower flux. In this study, composite membranes were prepared by cross-linking L-arginine and piperazine with trimesoyl chloride (1 and 0.5 %) (Singh et al. 2011). Membranes that were prepared using 0.5 % trimesoyl chloride with layer thickness of 0.4 μm exhibited a lower flux (Singh et al. 2011).

Dechlorination studies

One of the by-products formed during the dechlorination of 2,4,6-TCP is chloride ions (Fig. 8). The chloride ions generated by β-CD–G3-PSf-Fe/Ni were of lower concentration ($\sim$0.5 mg L^{-1}) than β-CD–G4-PSf-Fe/Ni ($\sim$1.5 mg L^{-1}) and remained at a constant concentration for the time tested. Low chlorine ions were reported by Schrick et al. (2002) for trichloroethylene dechlorination using Fe/Ni

Table 1 Water intake capacity, contact angle and pure water permeability for PSf, β-CD–PPI–PSf and β-CD–PPI–PSf-Fe/Ni membranes

Membranes	Water intake capacity (%)	Contact angle (°)	Porosity (%)	Pure water permeability (10^{-3} m h^{-1} MPa^{-1})	Thickness of surface layer (nm)
Commercial PSf	17	76	15	101	–
β-CD–G3-PPI–PSf	29	36	23	26	45
β-CD–G4-PPI–PSf	47	41	42	46	39
β-CD–G3-PSf-Fe/Ni	22	70	18	20	259
β-CD–G4-PSf-Fe/Ni	34	64	27	16	109

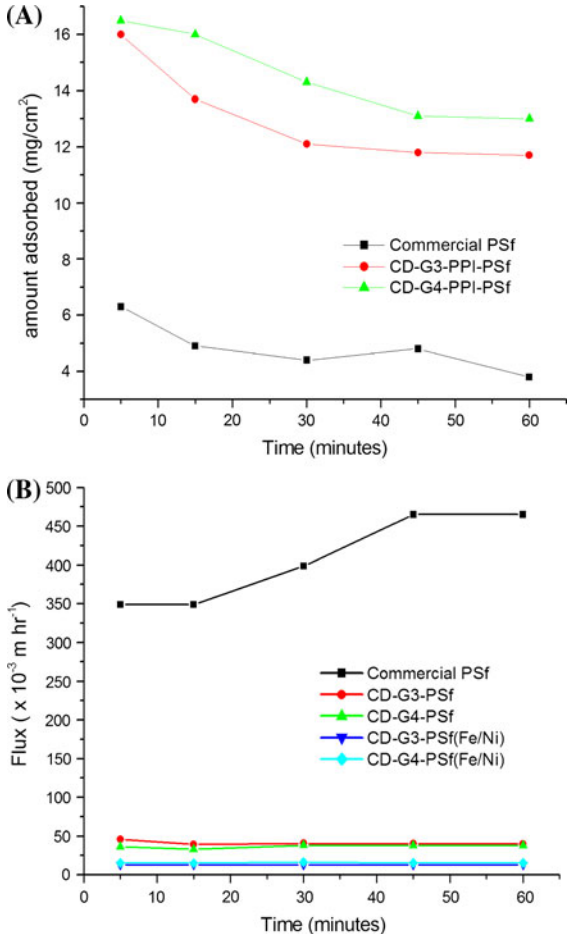

Fig. 6 **a** Adsorption efficiency of membranes overtime and **b** permeate flux at 0.69 MPa

nanoparticles. The low chloride ion concentration could be explained by the formation of insoluble chlorine containing hydroxides or adsorption of chloride by metal corrosion products (green rust) thus leading to low detection of the ion (Schrick et al. 2002). According to Smuleac et al. (2010), dechlorination reaction can be affected by two factors, i.e., iron oxide and Ni (or catalyst) deactivation due to coverage of oxide or hydroxides (Smuleac et al. 2010). Fe (0) can be corroded releasing ferrous ions and these ions cause an increase pH which in turn results in the formation of iron oxide (Yang et al. 2011; Meyer and Bhattacharyya 2007). The iron oxide deposits on the surface of the Fe (0) thus causing a decrease in dechlorination efficiency of the bimetallic system (Meyer and Bhattacharyya 2007: Yang et al. 2011). Therefore, the iron cannot produce hydrogen which can be deposited on the Ni to create active sites for dechlorination of 2,4,6-TCP. This can lower the dechlorination reactivity of the bimetallic Fe/Ni as seen for β-CD–G3-PSf-Fe/Ni membrane. Also as the 2,4,6-TCP is dechlorinated to other intermediate by-products, the nanocavities of the catalytic membranes maybe occupied by these molecules thus inhibiting further interaction of the 2,4,6-TCP with the catalytic membranes hence lowering dechlorination. This trend was also observed by Liu et al. (2010) where in situ photocatalytic regeneration of chitosan/activated carbon fibre/TiO_2 (CS/ACF/TiO_2) was affected by the presence of small molecules intermediate from oxidation of 2,4-dichlorophenol which inhibited the adsorption of 2,4-dichlorophenol onto the adsorption site of the CS/ACF/TiO_2 composite membrane.

To further confirm dechlorination, the permeate was analysed for the presence of other products using APCI-MS. The dechlorination products of 2,4,6-TCP were 4-chlorophenol (m/z 128.5), phenol ($m/z = 93.0$) and 2,4-dichlorophenol ($m/z = 162.9$) as illustrated in Fig. 9. Specifically for β-CD–G3-PSf-Fe/Ni 2,4-dichlorophenol was the only by-product detected after 60 min and for β-CD–G4-PSf-Fe/Ni, 4-chlorophenol (after 45 min) and phenol (after 60 min) were also detected. These products have also been reported by

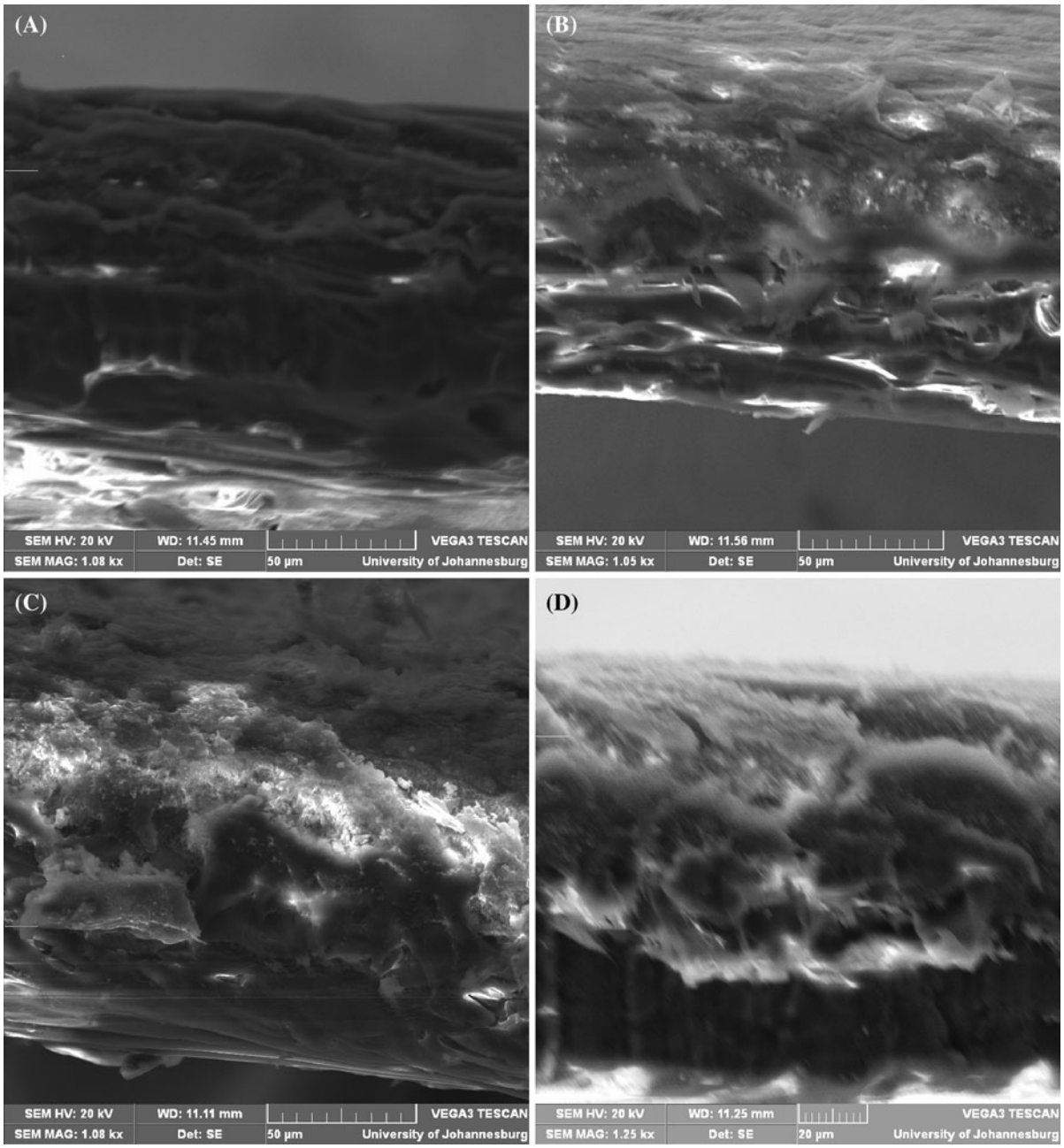

Fig. 7 Cross-section images for **a** β-CD–G3-PPI–PSf, **b** β-CD–G4-PPI–PSf, **c** β-CD–G3-PPI–PSf-NiFe, **d** β-CD–G4-PPI–PSf-NiFe

other researchers who have used different materials either for degradation or dechlorination of 2,4,6-TCP. Choi et al. (2007) detected phenol after reductive dechlorination of 2,4,6-TCP using a Fe/Pd-coated reactive barrier. Mun et al. (2008) used an acidogenic sequencing batch reactor to successfully dechlorinate 2,4,6-trichlorophenol to 4-chlorophenol. Gaya et al. (2010) used ZnO powder for the photocatalytic degradation of 2,4,6-trichlophenol, gas chromatography–mass spectrometry and high performance-liquid chromatography revealed the presence of 4-chlorophenol and phenol as the degradation intermediates and complete minerilisation of these intermediates was observed after 120 min.

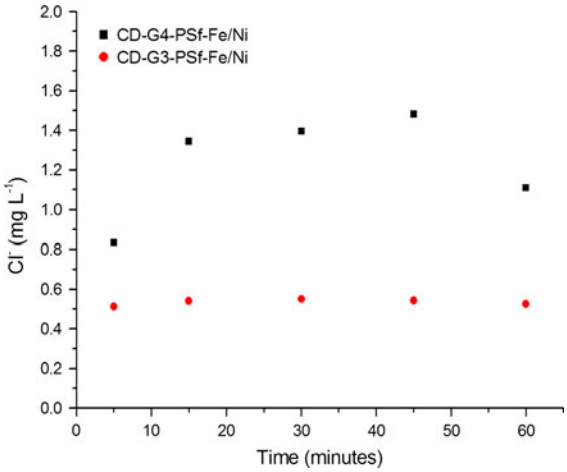

Fig. 8 Concentration of chlorine ions as a function of time for the dechlorination of 2,4,6-TCP under convection mode using β-CD–G3-PSf-Fe/Ni and β-CD–G4-PSf-Fe/Ni

Kinectic studies for the dechlorination of 2,4,6-TCP using batch studies

Data for kinetic evaluation based on the convective mode analysis were not used since the rate constant calculations are based on assumptions as reported by other investigators (Smuleac et al. 2010, 2011). Therefore, in this study we opted for the batch analysis to calculate the rate of the reaction and this was evaluated using Eq. 5 (Kuvarega et al. 2011) (Meyer and Bhattacharyya 2007):

$$\ln \frac{C}{C_0} = k_{\text{obs}} t \tag{5}$$

where k is the observed reaction rate constant, C and C_0 represent the concentration at initial time and time t, respectively. The values of k_{obs} obtained from the linear fit of the data are shown in Fig. 10. The rate constants for the dechlorination of 2,4,6-TCP was found to be 0.0015 and 0.0025 min^{-1} for β-CD–G3-PSf-Fe/Ni and β-CD–G4-PSf-Fe/Ni, respectively. These rate constants were found to be comparable with those reported by researchers who have prepared Ni/Fe nanoparticles using cellulose acetate membranes (Meyer and Bhattacharyya 2007). Meyer and Bhattacharyya (2007) reported a reaction rate constant of 0.29 h^{-1} (0.00483 min^{-1}) for the dechlorination of trichloroethylene for Fe/Ni nanoparticles embedded on cellulose acetate membranes which were prepared by phase inversion.

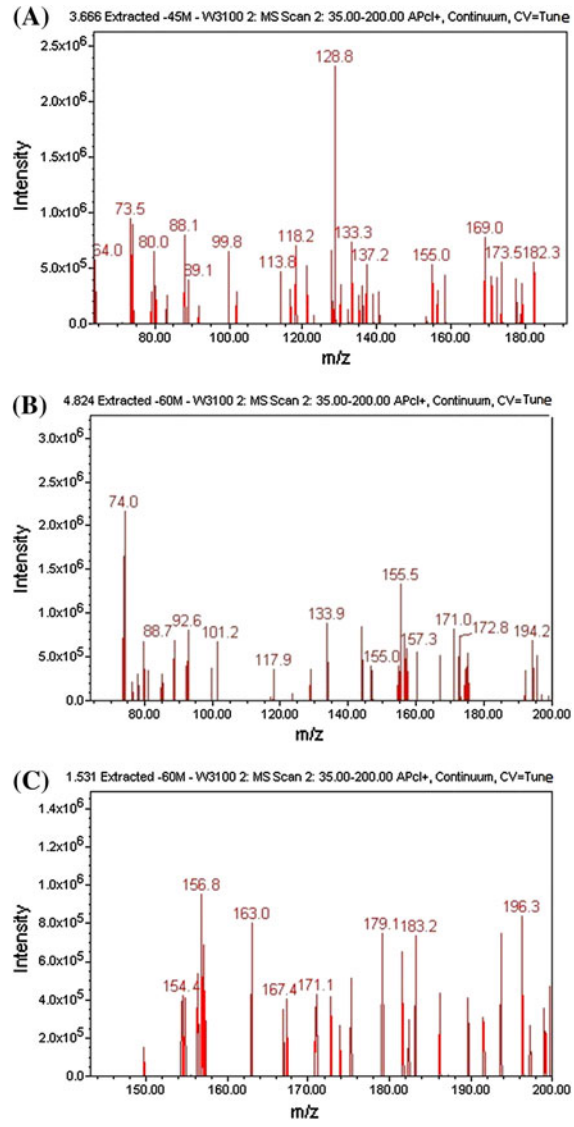

Fig. 9 APCI-MS analysis of 2,4,6-TCP dechlorination products **a** 4-chlorophenol, **b** phenol, **c** 2,4-dichlorophenol

Conclusion

The current study reports for the first time the synthesis of Fe/Ni nanoparticles in the presence of the β-cyclodextrin–dendrimer. HR-TEM demonstrated even distribution of the Fe/Ni nanoparticles and this feature is very important in the dechlorination of organic compounds such as 2,4,6-TCP. Dechlorination efficiency towards 2,4,6-TCP was comparable with other studies for the catalytic membranes and the presence of chloride ions, phenol, 4-chlorophenol and

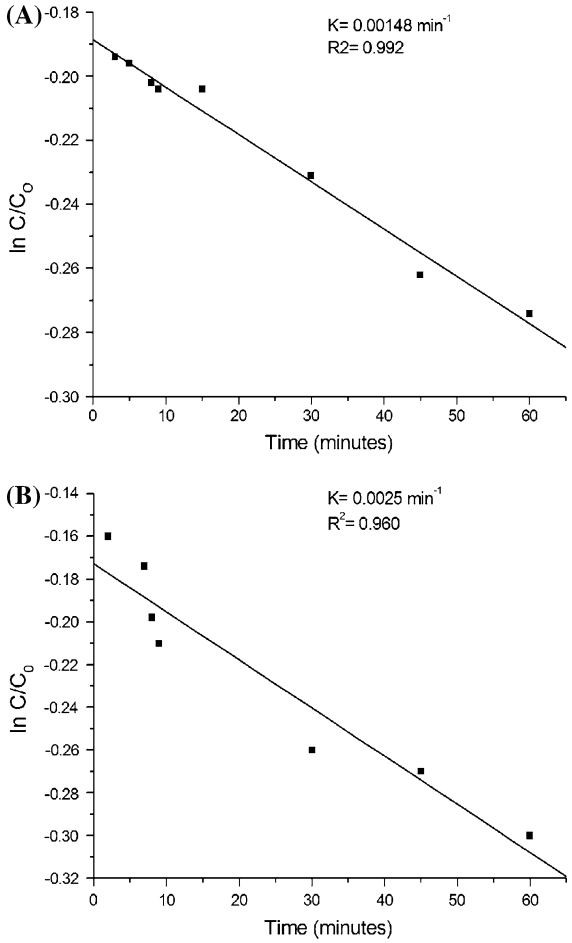

Fig. 10 Kinetics for the dechlorination of 2,4,6-TCP using β-CD–G3-PSf-Fe/Ni (**a**) and β-CD–G4-PSf-Fe/Ni (**b**)

2,4-dichlorophenol as by-products indicated that the membrane is feasible as a support for Fe/Ni nanoparticles.

Acknowledgments The author would like to thank the University of Johannesburg new generation scholarship for funding.

References

Abedini R, Mousavi SM, Aminzadeh R (2011) A novel cellulose acetate membrane using TiO2 nanoparticles: preparation, characterisation and permeation studies. Desalination 277:40–45

Adams FV, Nxumalo EN, Krause RWM, Hoek EMV, Mamba BB (2012) Preparation and characterization of polysulfone/β-cyclodextrin polyurethane composite nanofiltration membranes. J Membr Sci 405–406:291–299

Bai L, Wan H, Street SC (2009) Preparation of ultrafine FePt nanoparticles by chemical reduction in PAMAM-OH template. Coll Surf A 349:23–28

Bao C, Jin M, Lu R, Zhang T, Zhao YY (2003) Preparation of Au nanoparticles in the presence of low generational poly (amidoamine) dendrimer with surface hydroxyl groups. Mater Chem and Phys 81:160–165

Choi J, Kim Y, Choi SJ (2007) Reductive dechlorination and biodegradation of 2,4,6-trichlorophenol using sequential permeable reactive barriers: laboratory studies. Chemosphere 67:1551–1557

Diallo MS, Christie S, Swaminathan P, Jnr Johnson JH, 111 Goddard WA (2005) Dendrimer enhanced ultrafiltration.1. Recovery of Cu (II) from aqueous solutions using PAMAM dendrimers with ethylene diamine core and terminal NH_2 groups. Environ Sci Technol 39:1366–1377

Gaya UB, Abdullah AH, Hussein MZ, Zainal Z (2010) Photocatalytic removal of 2,4,6-trichlorophenol from water exploiting commercial ZnO powder. Desalination 263:176–182

Huang W, Kuhn JN, Tsung C, Zhang Y, Habas SE, Yang P, Somorjai GA (2008) Dendrimer templated synthesis of one nanometer Rh and Pt particles supported on mesoporous silica: catalytic activity for ethylene and pyrrole hydrogenation. Nano Lett 8:2027–2034

Jin XUE, Huang X, Hoek EMV (2009) Role of specific ion interactions in seawater RO membrane fouling by alginic acid. Environ Sci Technol 43:3580–3587

Kuvarega AT, Krause RWM, Mamba BB (2011) Nitrogen/palladium-codoped TiO_2 for efficient visible light photocatalytic dye degradation. J Phys Chem C 115:22110–22120

Lee HS, Im SJ, Kim JH, Kim HJ, Kim JP, Min BR (2008) Polyamide thin-film nanofiltration membranes containing TiO_2 nanoparticles. Desalination 219:48–56

Li N, Wei X, Mei Z, Xiong X, Chen S, Ye M, Ding S (2011) Synthesis and characterization of a novel polyamidoamine–cyclodextrin crosslinked copolymer. Carbohydr Res 346:1721–1727

Lianchao L, Baoguo W, Huimin T, Tianlu C, Jiping X (2006) A novel nanofiltration membrane prepared with PAMAM and TMC by in situ interfacial polymerization on PEK-C ultrafiltration membrane. J Membr Sci 269:84–93

Liu LF, Zhang PH, Yang FL (2010) Adsorptive removal of 2 4-DCP from water by fresh or regenerated chitosan/ACF/TiO_2 membrane. Sep Purif Technol 70:354–361

Malinga SP, Arotiba OA, Krause RW, Mapolie SF, Mamba BB (2012) Synthesis and characterisation of generation 2 and 3 poly(propyleneimine) dendrimer capped nanoalloy. Mater Lett 68:324–326

Meyer DE, Bhattacharyya D (2007) Impact of membrane immobilization on particle formation and trichloroethylene dechlorination for bimetallic Fe/Ni nanoparticles in cellulose acetate membranes. J Phys Chem B 111:7142–7154

Mun CH, Ng WJ, He J (2008) Acidogenic sequencing batch reactor start-up procedures for induction of 2,4,6-trichlorophenol dechlorination. Water Res 42:1675–1683

Park S, Cheedrala K, Diallo MS, Kim C, Kim IS, Goddard AW (2012) Nanofiltration membranes based on polyvinylidene fluoride nanofibrous scaffolds and crosslinked polyethyleneimine networks. J Nanopart Res. doi:10.1007/s11051-012-0884-7

Sarkar A, Carver PI, Zhang T, Merrington A, Bruza KJ, Rousseau JL, Keinath SE, Dvornic PR (2010) Dendrimer-based coatings for surface modification of polyamide reverse osmosis membranes. J Membr Sci 349:421–428

Schrick B, Blough JL, Jones AD, Mallouk TE (2002) Hydrodechlorination of trichloroethylene to hydrocarbons using bimetallic nickel-iron nanoparticles. Chem Mater 14:5140–5147

Scott RWJ, Wilson OM, Oh S, Kenik EA, Crooks RM (2004) Bimetallic palladium–gold dendrimer-encapsulated catalysts. J Am Chem Soc 4:7448–7453

Singh K, Ingole PG, Bhrambhatt H, Bhattachayra A, Bajaj HC (2011) Preparation, characterization and performance evaluation of chiral selective composite membranes. Sep Purif Technol 78:138–146

Smuleac V, Bachas L, Bhattacharyya D (2010) Aqueous-phase synthesis of PAA in PVDF membrane pores for nanoparticle synthesis and dichlorobiphenyl degradation. J Membr Sci 346:310–317

Smuleac V, Varma R, Sikdar S, Bhattacharyya D (2011) Green synthesis of Fe and Fe/Pd bimetallic nanoparticles in membranes for reductive degradation of chlorinated organics. J Membr Sci 379:131–137

Vassilev K, Turmanova S, Dimitrova M, Boneva S (2009) Poly (propylene imine) dendrimer complexes as catalysts for oxidation of alkenes. Eur Polym J 45:2269–2278

Wei X, Zhu L, Deng H, Xu Y, Zhu B, Huang Z (2008) New type of nanofiltration membrane based on crosslinked hyperbranched polymers. J Membr Sci 323:278–287

Weir M, Knecht M, Frenkel A, Crooks R (2010) Structural analysis of PdAu dendrimer-encapsulated bimetallic nanoparticles. Langmuir 26:1137–1146

Xu J, Dozier A, Bhattacharyya D (2005) Synthesis of nanoscale bimetallic particles in polyelectrolyte membrane matrix for reductive transformation of halogenated organic compounds. J Nanopart Res 7:449–467

Yang L, Lv L, Zhang S, Pan B, Zhang W (2011) Catalytic dechlorination of monochlorobenzene by Pd/Fe nanoparticles immobilized within a polymeric anion exchanger. Chem Eng J 178:161–167